PNAS
www.pnas.org

Supplementary Information for

Ketamine can produce oscillatory dynamics by engaging mechanisms dependent on the kinetics of NMDA receptors

Elie Adam, Marek Kowalski, Oluwaseun Akeju, Earl K. Miller, Emery N. Brown, Michelle M. McCarthy, and Nancy Kopell

Correspondence should be addressed to E.A., M.M. and N.K.
E-mail: eadam@mit.edu, mmccart@bu.edu and nk@bu.edu.

This PDF file includes:

Supporting Information Text

The supplementary text contains all the methods and details on the biophysical modeling. All neurons were modeled using a single compartment with Hodgkin-Huxley-type dynamics. The voltage change in each neuron is described by:

$$c_m \frac{dv}{dt} = -\sum I_{membrane} - \sum I_{synaptic} + I_{app} + I_{noise} \quad [1]$$

The membrane capacitance (c_m) is normalized to 1 μF$\cdot cm^{-2}$ for all neurons. All neurons display a fast sodium current (I_{Na}), a fast potassium current (I_k), a leak current (I_L) for membrane currents ($I_{membrane}$). The synaptic currents ($I_{synaptic}$) depend on the connectivity. The applied current (I_{app}) is a constant that represents background excitation and the noise current (I_{noise}) corresponds to a gaussian noise. The parameter values for PYR, IN-Phasic and IN-Tonic neurons generally follow the parameter values for excitatory and inhibitory neurons in (1) and (2). They have been derived from experimental findings in the literature, as cited in previous work such as (1, 2, 13). Any parameter value not within the ranges in (1) and (2) is justified when it is introduced, below.

Membrane currents and background excitation

The basic membrane currents were modeled using Hodgkin-Huxley-type conductance dynamics and formulated as:

$$I = \bar{g}(m^n h^k)(V - E_{ion}) \quad [2]$$

Every membrane current has a constant maximal conductance ($\bar{g}$) and a constant reversal potential (E_{ion}). The activation (m) and inactivation (h) gating variables have n^{th} and k^{th} order kinetics with $n, k \geq 0$. The dynamics of each gating variable evolves according to the kinetic equation (written here for the gating variable m):

$$\frac{dm}{dt} = \frac{m_\infty - m}{\tau_m} \quad [3]$$

The steady-state function (m_∞) and the time constant of decay (τ_m) can be formulated as rate functions for each opening (α_m) and closing (β_m) of the ionic channel by using:

$$m_\infty = \alpha_m/(\alpha_m + \beta_m) \quad \text{and} \quad \tau_m = 1/(\alpha_m + \beta_m). \quad [4]$$

Fast sodium current. The sodium current (I_{Na}) has three activation gates (n=3) and only one inactivation gate (k=1). The rate functions for the sodium current activation (m) and inactivation (h) variables are formulated as:

$$\alpha_m = \frac{0.32(V+54)}{1-\exp[-(V+54)/4]} \quad [5]$$

$$\beta_m = \frac{0.28(V+27)}{\exp[(V+27)/5]-1} \quad [6]$$

$$\alpha_h = 0.128\exp[-(V+50)/18] \quad [7]$$

$$\beta_h = \frac{4}{1+\exp[-(V+27)/5]} \quad [8]$$

The maximal conductance of the sodium current is $\bar{g}_{Na} = 100$ mS$\cdot$cm^{-2}. The sodium reversal potential is $E_{Na} = 50$mV.

Fast potassium current. The fast potassium current (I_K) has four activation gates ($n = 4$) and no inactivation gates ($k = 0$). The rate functions of the activation gate are described by:

$$\alpha_m = \frac{0.032(V+52)}{1-\exp[-(V+52)/5]} \quad [9]$$

$$\beta_m = 0.5\exp[-(V+57)/40] \quad [10]$$

The maximal fast potassium channel conductance is $\bar{g}_K = 80$ mS$\cdot$cm^{-2}. The reversal potential for potassium is $E_K = -100$mV.

Leak current. The leak current (I_L) has no gating variables ($n = 0$, $k = 0$). The maximal conductance of the leak channel is $\bar{g}_l = 0.05$ mS$\cdot$cm^{-2}. The leak channel reversal potential is $E_L = -67$mV.

Applied current and noise. The baseline excitation and the sum of all excitatory and inhibitory exogenous inputs for a given neuron (e.g., from the cortex, thalamus and non-modeled input) is introduced into the model using a constant background excitation term (I_{app}). To account for variability in background excitation, we further introduce a Gaussian noise term (I_{noise}). The Gaussian noise has mean zero and standard deviation dependent on the neuronal cell type. The applied current (I_{app}) is set to -0.25 μA$\cdot cm^{-2}$ for PYR neurons, 0.1 μA$\cdot cm^{-2}$ for IN-Phasic neurons, and -1.4 μA$\cdot cm^{-2}$ for IN-Tonic neurons. The Gaussian noise (I_{noise}) has mean 0 and standard deviation $20\sqrt{0.01}$ for PYR and IN-Phasic neurons and $150\sqrt{0.01}$ for IN-Tonic neurons where 0.01ms corresponds to the time step of integration in our simulations.

Network structure and synaptic currents

Our model consisted of 80 PYR, 20 IN-Phasic, and 80 IN-Tonic neurons. Each PYR neuron receive 10 AMPA+NMDA projections from the remaining 79 PYR neurons, 10 GABA projections from the 20 IN-Phasic neurons and 5 GABA projections from the 80 IN-Tonic neurons. Each IN-Phasic neuron receive 10 AMPA+NMDA projections from 80 PYR neurons, 10 GABA projections from the remaining 19 IN-Phasic neurons and 5 GABA projections from the 80 IN-Tonic neurons. IN-Tonic neurons receive no projections in the base model. All projections were randomly and uniformly selected for a total of 10 from each cell type.

We needed IN-Tonic inhibition onto PYR and IN-Phasic neurons that is heterogenous and random, that would not foster synchrony and that would not pattern the activity of PYR and IN-Phasic neurons. To achieve that, we opted to provide GABAergic projections from a relatively large pool (80) of IN-Tonic neurons, instead of a small pool (e.g., 20) with size similar to that of IN-Phasic neurons. Each PYR and IN-Phasic neuron received input from 5 IN-Tonic neurons. This ensure that neurons (PYR and IN-Phasic) do not excessively have presynaptic input from the same combination of IN-Tonic neurons. As IN-Tonic neurons are not interconnected, the size of the IN-Tonic population only affects the heterogeneity and randomness of the inhibition onto PYR and IN-Phasic neurons.

While IN-Tonic neurons do not receive projections in the base model, they are modeled to have NMDA-receptors. The concentration [Glu] for NMDA_R of IN-Tonic neurons were all fixed to 1mM to provide constant excitatory input, which would allow NMDA_R kinetics to open and close. The concentration [Glu] for NMDA_R for PYR and IN-Phasic neurons is derived from pre-synaptic activity, as described in the next subsection. We fixed the [Glu] concentration for IN-Tonic neurons to examine the slow-unblock current without closed-loop effects. However, the results are unchanged if that concentration is instead from pre-synaptic PYR activity (Fig. S6A).

NMDA-receptor kinetics and current. We implemented a 10-state probabilistic model of NMDA_R channel kinetics, adapted from (3). The probabilty of being a certain state can be interpreted as the fraction of NMDA receptors in the particular state. State i transitions to state j with a rate q_{ij}, denoting a conditional transition probability. The notation for the states and the rates are provided in Figure S8. If Q is the 10x10 transition matrix and $P(t)$ is the probability vector of being in each of the 10 states, then:

$$\frac{dP(t)}{dt} = Q.P(t) \quad [11]$$

For example, for the conductive state O_{AA}, we get:

$$\frac{d\text{O}_{\text{AA}}}{dt} = \beta \text{C}_{\text{Å}} + k_{\text{unblock}}(V)\text{O}_{\text{AA}} - \alpha \text{C}_{\text{AA}} - k_{\text{block}}(V)\text{O}_{\text{AA}} \quad [12]$$

The values for the rates are:

$$\alpha = 0.0916 \text{ ms}^{-1} \quad [13]$$

$$\beta = 0.0465 \text{ ms}^{-1} \quad [14]$$

$$k_{\text{unblock}}(V) = 5.4 \exp(V/47) \text{ ms}^{-1} \quad [15]$$

$$k_{\text{block}}(V) = 0.61 \exp(-V/17) \text{ ms}^{-1} \quad [16]$$

$$k_{\text{on}} = 5 \text{ mM.ms}^{-1} \quad [17]$$

$$k_{\text{off}} = 0.0055 \text{ ms}^{-1} \quad [18]$$

$$k_{\text{r}} = 0.0018 \text{ ms}^{-1} \quad [19]$$

$$k_{\text{d}} = 0.0084 \text{ ms}^{-1} \quad [20]$$

Built into the model of (3) is an asymmetry in the kinetics during the blocked versus unblocked regime. We decide to use a symmetric version of the model for simplicity and to have our results not depend on asymmetry. This distinction will not affect our results but, in general, can be a crucial component that can affect brain dynamics through NMDA-receptor kinetics. We also substituted the variable $[\text{Mg}]^{2+}$ that appears in the blocking/unblocking rates of (3) by 1mM (see (3)).

Each NMDA_R synaptic connection consists of such a probabilistic model. NMDA_R channels open following agonist (glutamate) binding. The concentration [Glu] denotes the amount of glutamate available at the synapse that can bind to NMDA receptors. Binding rates are determined by this concentration (Fig. S8). This concentration is given by:

$$[\text{Glu}] = [\text{Glu}]_{\text{max}} \exp(-t/\tau_{[\text{Glu}]}) \quad [21]$$

where t denotes the time of the last spike from the presynaptic neuron. We set $[\text{Glu}]_{\text{max}} = 1\text{mM}$ and $\tau_{[\text{Glu}]} = 1.2\text{ms}$. We then modeled the NMDA current (I_{NMDA}) as:

$$I_{NMDA} = g_{NMDA} s_{NDMA} (V - E_{NMDA}) \quad [22]$$

The gating variables s_{NDMA} is the sum:

$$s_{NMDA} = \frac{1}{N} \sum_{k=1}^{N} \text{O}_{\text{AA}(k \to j)} \quad [23]$$

where N is the number of presynaptic neurons and $O_{AA_{(k\to j)}}$ is the probability of being in state O_{AA} for $NMDA_R$ synaptic connection $k \to j$. The maximal conductance g_{NMDA} was set to be 8.5 mS·cm^{-2} for PYR neurons and 9.5 mS·cm^{-2} for IN-Phasic and IN-Tonic neurons. These values were chosen to preserve a reasonable NMDA-current/AMPA-current ratio as described in (4).

GABA- and AMPA-receptor currents. We modeled GABA-currents (I_{GABAa}) using a Hodgkin-Huxley-type conductance:

$$I_{GABAa} = \bar{g}_{inh} s_{inh} (V - E_{inh}) \quad [24]$$

of the gating variables from all pre-synaptic connections. The gating variable s_{inh} for inhibitory GABAa synaptic transmission is the sum:

$$s_{inh} = \frac{1}{N} \sum_{k=1}^{N} S_{k\to j} \quad [25]$$

where N is the number of presynaptic neurons and $S_{k\to j}$ describes the kinetics of the gating variable, for each pair of presynaptic neuron k and postsynaptic neuron j, evolving according to:

$$\frac{dS_{k\to j}}{dt} = g_{GABAa(V_k)}(1 - S_{k\to j}) - \frac{S_{k\to j}}{\tau_{inh}}. \quad [26]$$

Note that $S_{k\to j}$ is a function of the presynaptic voltage V_k, and its dynamics depend on the dynamics of the presynaptic neuron k. The rate functions for the open state of the GABAa receptor ($g_{GABAa}(V_k)$) is described by:

$$g_{GABAa}(V_k) = 2(1 + tanh(\frac{V_k}{4})). \quad [27]$$

The maximal conductance $\bar{g}_{inh}$ is scaled by the number of pre-synaptic neurons of the same type. Excitatory AMPA synaptic currents use the same set of equations as for the GABAa current with the "GABA" subscript replaced by "AMPA" and the "inh" subscript replaced by "exc", with the exception for $g_{AMPA}(V_k)$ modifed as $g_{AMPA}(V_k) = 5(1 + tanh(\frac{V_k}{4}))$.

We set τ_{inh} to be $6ms$ for projections from IN-Phasic neurons and $8ms$ for projections from IN-Tonic neurons. We set $\tau_{exc} = 1.5ms$ for all PYR projections. The potentials E_{inh} and E_{exc} were defined as $-80mV$ and $0mV$, respectively. Maximal conductances were $\bar{g}_{exc} = 0.2$ mS·cm^{-2} for AMPA-currents from PYR neurons, $\bar{g}_{inh} = 0.8$ mS·cm^{-2} for GABA-currents from IN-Phasic neurons and $\bar{g}_{inh} = 5$ mS·cm^{-2} for GABA-currents from IN-Tonic neurons.

The value of the maximal conductance for IN-Tonic GABA-currents was selected so that IN-Tonic neurons can deliver adequate inhibition onto PYR and IN-Phasic neurons: abolishing gamma oscillation that emerge from PYR and IN-Phasic neuron disinhibition while maintaining spiking activity in PYR and IN-Phasic neurons. The value (5 mS·cm^{-2}) appears to be much larger than that of IN-Phasic neurons (0.8 mS·cm^{-2}). However, each PYR and IN-Phasic neuron received projections from 5 IN-Tonic neurons. These IN-Tonic neurons fire randomly, sparsely and not simultaneously. This is as opposed to IN-Phasic neurons which become highly active and synchronized when disinhibited. As a result, the maximal value for the conductance of IN-Tonic GABAergic currents during simulations is effectively near 1 mS·cm^{-2}, the maximal conductance provided by each of the 5 IN-Tonic synaptic connections. Overall, the role of this IN-Tonic projection and its maximal conductance is to provide tonic inhibition onto PYR and IN-Phasic neurons to keep neuronal excitation low. These IN-Tonic GABAergic currents do not play a kinetic role in the generation of the gamma and slow-delta oscillations.

Extended model with VIP neurons

We added 20 VIP neurons in an extended model. The properties and currents of these neurons can differ from what was already detailed above. The additions or changes are described below. The parameters for VIP neurons follow those presented for VIP in (5) and for fast spiking interneurons in (6).

Modifications to membrane potentials. The fast sodium channel maximal conductance was set to $\bar{g}_{Na} = 112.5$ mS·cm^{-2} for VIP neurons. VIP neurons also displayed a D-current, an M-current and a modified fast potassium current.

Fast potassium current for VIP+ neurons. The fast potassium current for VIP+ (I_K) has two activation gates (n=2) and no inactivation gate (k=0). The steady state function for the potassium current activation (n) and its constant (τ_n) are described by:

$$n_\infty = \frac{1}{1 + \exp[-(V + 12.4)/6.8]} \quad [28]$$

$$\tau_n = (0.087 + \frac{11.4}{1 + \exp[(V + 14.6)/8.6]})(0.087 + \frac{11.4}{1 + \exp[-(V - 1.3)/18.7]}) \quad [29]$$

The maximal conductance of the potassium current is $\bar{g}_K = 225$ mS·cm^{-2}. The potassium reversal potential is $E_{Na} = -90$mV. This instantiation of the current is only displayed in VIP neurons.

D-current. The fast-activating, slowly inactivating potassium D-current (I_D) is described mathematically as in (7) and has three activation gates (n = 3) and one inactivation (k = 1) gate. The steady state functions for the activation (m) and inactivation (h) variables and their time constants (τ_m and τ_h, respectively) are described by:

$$m_\infty = \frac{1}{1+\exp[-(V+50)/20]} \quad [30]$$

$$h_\infty = \frac{1}{1+\exp[(V+70)/6]} \quad [31]$$

$$\tau_m = 2\text{ms} \quad [32]$$

$$\tau_h = 150\text{ms} \quad [33]$$

The maximal conductance of the D-current is 5.6 mS·cm^{-2} for VIP.

M-current. The M-current (I_M) has one activation gate ($n = 1$) and no inactivation gate ($k = 0$). The rate functions for the M-current activation gate are described by:

$$\alpha_m = \frac{Q_s 10^{-4}(V+30)}{1-\exp[-(V+30)/9]} \quad [34]$$

$$\beta_m = -\frac{Q_s 10^{-4}(V+30)}{1-\exp[(V+30)/9]} \quad [35]$$

We use a Q_{10} factor of 2.3 to scale the rate functions of the M-current since the original formulation of these kinetics described dynamics at $23^\circ C$ (8). Thus, for a normal body temperature of $37^\circ C$, the M-current rate equations are scaled by Q_s, which is formulated as:

$$Q_s = Q_{10}^{(37^\circ C - 23^\circ C)/10} = 3.209 \quad [36]$$

The maximal M-current conductance is $\bar{g_m} = 1.3$ mS·cm^{-2} for VIP.

Leak current. The maximal conductance of the leak channel is $\bar{g_l} = 0.025$ mS·cm^{-2} for VIP. The leak channel reversal potential is $E_L = -70$mV for VIP.

Applied current and noise. The applied current (I_{app}) is set to 5 μA·cm^{-2} for VIP. The Gaussian noise (I_{noise}) has mean 0 and standard deviation $100\sqrt{0.01}$ for VIP where 0.01ms corresponds to the time step of integration in our simulations.

Modifications to connectivity. Maximal conductances was $\bar{g}_{inh} = 0.3$ mS·cm^{-2} for GABA-currents from VIP projections and $\bar{g}_{inh} = 1$ mS·cm^{-2} for AMPA-currents from PYR projections.

Gap junctions. VIP neurons were additionally connected via electrical gap junctions. The electrical coupling of VIP neuron j to neuron k was defined as:

$$I_{elec} = \frac{1}{N}\bar{g}_{elec}(V_k - V_j) \quad [37]$$

with N equal to the number of VIP neurons that j is coupled to. These coupling introduce a current $\sum_k I_{elec}$ in VIP neuron j. We set $\bar{g}_{elec} = 0.4$ mS·cm^{-2}

Network and connectivity. Each VIP neuron receive 10 AMPA projections from PYR neurons and 10 GABA projections from VIP+ neurons. Each VIP+ neuron is also coupled to 10 remaining VIP neurons. All the projections are randomized. The projections received by PYR and IN-Phasic neurons are uniformly selected for a total of 10 from each cell type. The projections received by VIP+ neurons are selected by a bernouilli coin flip of probability 0.125 for AMPA projections from PYR neurons, 0.5 for GABA projections from VIP neurons, 0.5 for electrical coupling from VIP neurons. The electrical coupling of VIP+ neurons was made symmetrical.

Modeling the effect of ketamine

The effect of ketamine was modeled by decreasing $k_{\text{unblock}}(0)$ from 5.4 ms^{-1} at baseline by 15% 4.6 ms^{-1} and then by 30% to 3.8 ms^{-1} at the highest dose. This decrease was applied to all NMDA receptors of all the neurons in the network.

Network perturbation simulations

An isolated PYR neuron for NMDA$_R$ kinetics simulations was formed by removing all projections, and setting [Glu] = 1 and letting it decay per the equation to simulate a glutamate puff. The applied current I_{app} was set to -2 μA·cm^{-2}, -1.25 μA·cm^{-2} and -0.5 μA·cm^{-2} in Figure 4B,C (top to bottom). The applied current I_{app} was set to -0.5 μA·cm^{-2} and $k_{\text{unblock}}(0)$ decreased from 5.4ms to 3.8ms in Figure 5B,C (top to bottom).

In Figures 4F and 5G, I_{app} increased to 0.15 μA·cm^{-2} for PYR neurons and to 0.6 μA·cm^{-2} for IN-Phasic neurons. In Figure S6C, I_{app} was decreased to -2.05 μA·cm^{-2} and E_l was increased to $-53mV$. In Figure S7B, I_{app} was decreased to -1.4 μA·cm^{-2}. In Figure S7C [Glu]was fixed to 0.5mM, and I_{app} was decreased to -0.9 μA·cm^{-2}.

Aggregate population activity

Synaptic currents have been used in models of LFP and EEG (9). We model the population aggregate activity (EEG/LFP) as the sum of all AMPA and NMDA currents going into PYR neurons. Thus our aggregate signal is tracking the excitatory activity driving spiking throughout the network.

Simulation and analysis

Our network models were programmed in C++ and compiled using GNU gcc. The differential equations were integrated using a fourth-order Runge Kutta algorithm. The integration time step was 0.01 ms. Model output is graphed and analyzed using Python 3. Signals were filtered using a butterworth band-pass filter of order 2.

References

1. S Ching, A Cimenser, PL Purdon, EN Brown, NJ Kopell, Thalamocortical model for a propofol-induced α-rhythm associated with loss of consciousness. *Proc. Natl. Acad. Sci.* **107**, 22665–22670 (2010).
2. E Adam, O Kwon, KA Montejo, EN Brown, Modulatory dynamics mark the transition between anesthetic states of unconsciousness. *Proc. Natl. Acad. Sci.* **120**, e2300058120 (2023).
3. M Vargas-Caballero, HP Robinson, Fast and slow voltage-dependent dynamics of magnesium block in the nmda receptor: the asymmetric trapping block model. *J. Neurosci.* **24**, 6171–6180 (2004).
4. CI Myme, K Sugino, GG Turrigiano, SB Nelson, The nmda-to-ampa ratio at synapses onto layer 2/3 pyramidal neurons is conserved across prefrontal and visual cortices. *J. neurophysiology* **90**, 771–779 (2003).
5. A Cattani, DB Arnold, M McCarthy, N Kopell, Basolateral amygdala oscillations enable fear learning in a biophysical model. *eLife* **12** (2023).
6. EM Adam, EN Brown, N Kopell, MM McCarthy, Deep brain stimulation in the subthalamic nucleus for parkinson's disease can restore dynamics of striatal networks. *Proc. Natl. Acad. Sci.* **119**, e2120808119 (2022).
7. D Golomb, et al., Mechanisms of firing patterns in fast-spiking cortical interneurons. *PLoS Comput. Biol.* **3**, e156 (2007).
8. ZF Mainen, TJ Sejnowski, Influence of dendritic structure on firing pattern in model neocortical neurons. *Nature* **382**, 363–366 (1996).
9. MM McCarthy, EN Brown, N Kopell, Potential network mechanisms mediating electroencephalographic beta rhythm changes during propofol-induced paradoxical excitation. *J. Neurosci.* **28**, 13488–13504 (2008).

Supplementary Figures

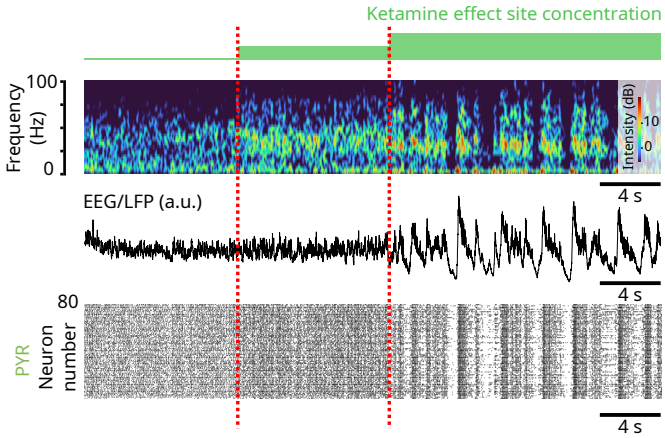

Fig. S1. Simulation 1: NMDA$_R$ antagonism in a biophysical model reproduces the oscillatory dynamics under ketamine. (Model simulations) (top) Spectrogram of an EEG/LFP generated from a simulation of the biophysical model, under different effect site concentrations of ketamine. (middle) Corresponding EEG/LFP trace. (bottom) Corresponding raster plot of spiking activity.

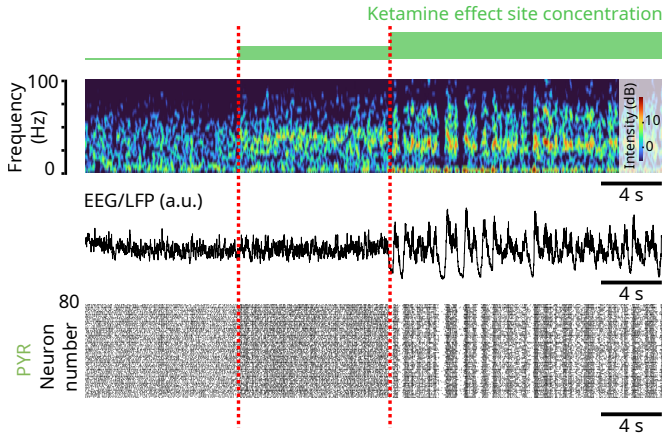

Fig. S2. Simulation 2: $NMDA_R$ antagonism in a biophysical model reproduces the oscillatory dynamics under ketamine. (Model simulations) (top) Spectrogram of an EEG/LFP generated from a simulation of the biophysical model, under different effect site concentrations of ketamine. (middle) Corresponding EEG/LFP trace. (bottom) Corresponding raster plot of spiking activity.

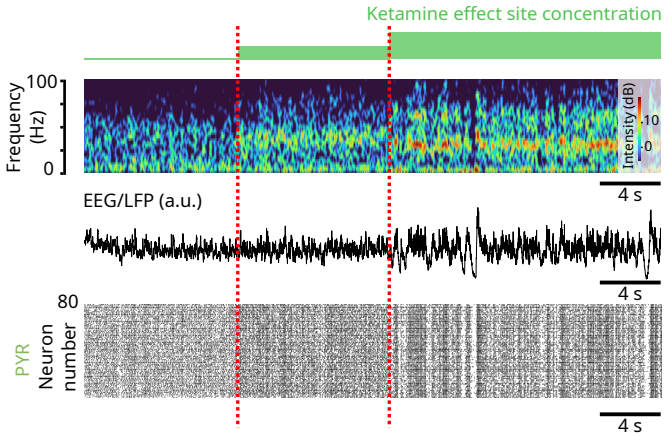

Fig. S3. Simulation 3: NMDA$_R$ antagonism in a biophysical model reproduces the oscillatory dynamics under ketamine. (Model simulations) (top) Spectrogram of an EEG/LFP generated from a simulation of the biophysical model, under different effect site concentrations of ketamine. (middle) Corresponding EEG/LFP trace. (bottom) Corresponding raster plot of spiking activity.

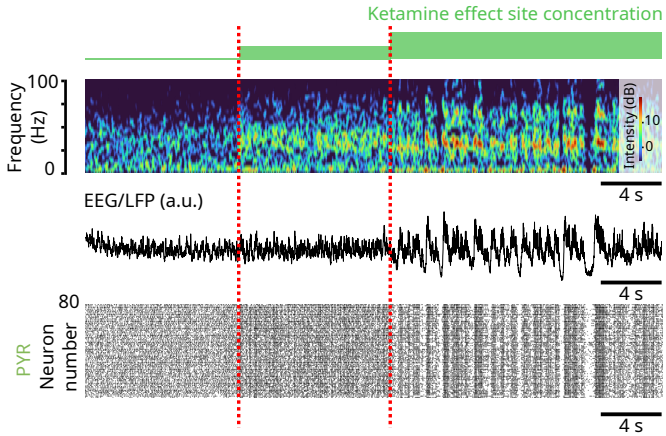

Fig. S4. Simulation 4: NMDA$_R$ antagonism in a biophysical model reproduces the oscillatory dynamics under ketamine. (Model simulations) (top) Spectrogram of an EEG/LFP generated from a simulation of the biophysical model, under different effect site concentrations of ketamine. (middle) Corresponding EEG/LFP trace. (bottom) Corresponding raster plot of spiking activity.

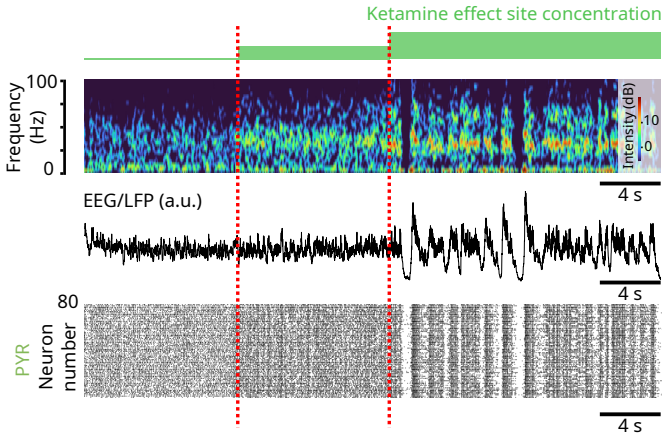

Fig. S5. Simulation 5: NMDA$_R$ antagonism in a biophysical model reproduces the oscillatory dynamics under ketamine. (Model simulations) (top) Spectrogram of an EEG/LFP generated from a simulation of the biophysical model, under different effect site concentrations of ketamine. (middle) Corresponding EEG/LFP trace. (bottom) Corresponding raster plot of spiking activity.

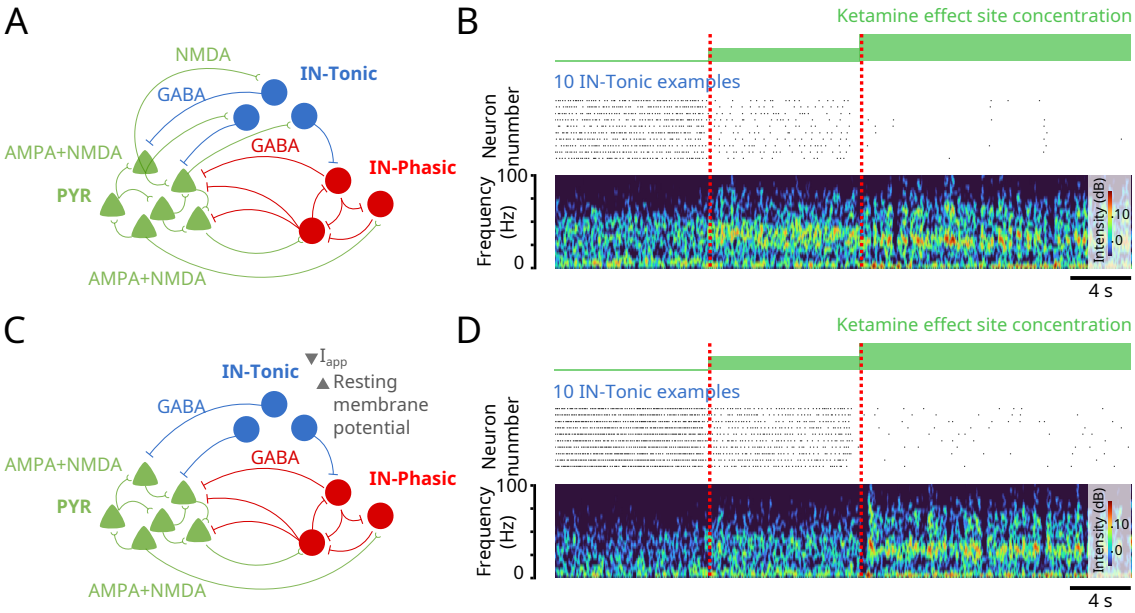

Fig. S6. NMDA$_R$ antagonism can shut down inhibition under different conditions. (Model simulations) (A) Schematic of the biophysical model with added NMDA projections from PYR to IN-Tonic neurons. **(B)** (top) Raster plot of spiking activity of representative IN-Tonic neurons. (bottom) Spectrogram of an LFP generated from a simulation of the biophysical model of (A), under different effect site concentrations of ketamine. **(C)** Schematic of the biophysical model where the background excitation is decreased and the resting membrane potential is increased. **(D)** (top) Raster plot of spiking activity of representative IN-Tonic neurons. (bottom) Spectrogram of an LFP generated from a simulation of the biophysical model of (C), under different effect site concentrations of ketamine.

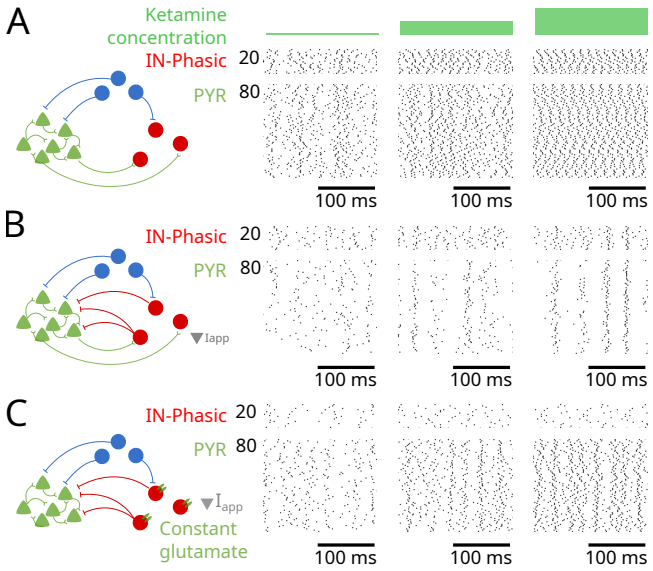

Fig. S7. Effects of GABA-receptor inhibition on gamma oscillations under NMDA$_R$ antagonism. (Model simulations) (A) (left) Schematic of the network for the simulation where IN-PYR and IN-IN projections were removed. (right) Raster plots of spiking activity for IN-Phasic and PYR neurons under the conditions in (left), at different ketamine effect site concentrations. **(B)** (left) Schematic of the network for the simulation where IN-IN projections were removed and Iapp adjusted accordingly to correct increase in excitation. (right) Raster plots of spiking activity for IN-Phasic and PYR neurons under the conditions in (left), at different ketamine effect site concentrations. **(C)** (left) Schematic of the network for the simulation where IN-IN and PYR-IN projections were removed. NMDA$_R$ on IN were exposed to constant glutamate concentration, and Iapp was decreased to correct for increase of excitation. (right) Raster plots of spiking activity for IN-Phasic and PYR neurons under the conditions in (left), at different ketamine effect site concentrations.

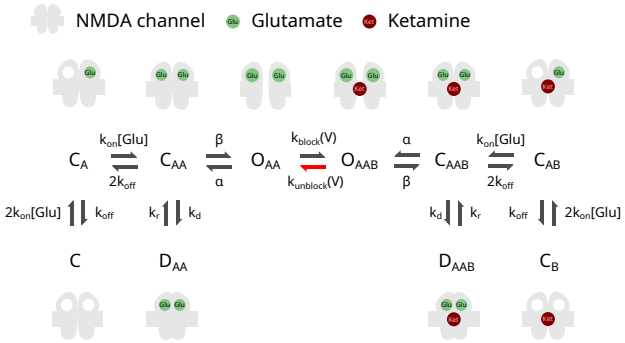

Fig. S8. Transitions in the 10-state probabilistic model of NMDA$_R$ kinetics. Schematic of the 10-state model of NMDA$_R$ kinetics displaying the variables for the transition rates.